REPORT DOCUMENTATION PAGE

Form Approved
OMB No. 0704-0188

1. REPORT DATE *(DD-MM-YYYY)*	**2. REPORT TYPE**	**3. DATES COVERED** *(From - To)*
June 2014	Technical Paper	June 2014- July 2014

4. TITLE AND SUBTITLE

Receptivity of a Cryogenic Coaxial Gas-Liquid Jet to Acoustic Disturbances

5a. CONTRACT NUMBER
In-house

5b. GRANT NUMBER

5c. PROGRAM ELEMENT NUMBER

6. AUTHOR(S)

Wegener, J; Forliti, D; Leyva, I; Talley, D

5d. PROJECT NUMBER

5e. TASK NUMBER

5f. WORK UNIT NUMBER
Q0YA

7. PERFORMING ORGANIZATION NAME(S) AND ADDRESS(ES)

Air Force Research Laboratory (AFMC)
AFRL/RQRC
10 E. Saturn Blvd.
Edwards AFB CA 93524-7680

8. PERFORMING ORGANIZATION REPORT NO.

9. SPONSORING / MONITORING AGENCY NAME(S) AND ADDRESS(ES)
Air Force Research Laboratory (AFMC)
AFRL/RQR
5 Pollux Drive
Edwards AFB CA 93524-7048

10. SPONSOR/MONITOR'S ACRONYM(S)

11. SPONSOR/MONITOR'S REPORT NUMBER(S)
AFRL-RQ-ED-TP-2014-159

12. DISTRIBUTION / AVAILABILITY STATEMENT
Distribution A: Approved for Public Release; Distribution Unlimited

13. SUPPLEMENTARY NOTES
Technical paper presented at 50th AIAA/ASME/SAE/ASEE Joint Propulsion Conference, Cleveland, OH, 28-30 July, 2014.
PA#14311

14. ABSTRACT

An experimental study has been conducted at the Air Force Research Laboratory at Edwards Air Force Base to explore the receptivity of cryogenic coaxial jet flows to transverse acoustic disturbances. The shear coaxial jet flow employed liquid nitrogen in the inner jet and cooled helium in the outer annular jet to represent the nominal fluid dynamical conditions of an oxygen/hydrogen liquid rocket engine injector. The injector flow is submerged in a chamber that experiences a monotonic transverse acoustic resonance characteristic of a rocket chamber in the presence of combustion instability. The coaxial jet is exposed to a variety of acoustic conditions including different frequencies, amplitudes, and locations within the resonant mode shape. High-speed back-lit images were captured to record the behavior of the natural (unforced) and forced coaxial jets. Proper orthogonal decomposition and spectral analysis were used to extract natural and forced modes. Convective modes are extracted, and a new Strouhal number is used to characterize the dominant natural convective mode that is analogous to the preferred mode in free jets. The threshold of receptivity was found for a number of different injector flows and acoustic forcing conditions. The results indicate that the dimensionless frequency plays an important role, and there exists a finite forcing amplitude at which the threshold of receptivity occurs. The receptivity threshold and post receptivity response provides useful insight on the suitability of a given injector design for specific rocket combustion chamber conditions.

15. SUBJECT TERMS

16. SECURITY CLASSIFICATION OF:			**17. LIMITATION OF ABSTRACT**	**18. NUMBER OF PAGES**	**19a. NAME OF RESPONSIBLE PERSON**
					Doug Talley
a. REPORT	**b. ABSTRACT**	**c. THIS PAGE**	SAR	14	**19b. TELEPHONE NO** *(include area code)*
Unclassified	**Unclassified**	**Unclassified**			661-275-6174

Standard Form 298 (Rev. 8-98)
Prescribed by ANSI Std. 239.18

Receptivity of a Cryogenic Coaxial Gas-Liquid Jet to Acoustic Disturbances

Jeffrey L. Wegener[1]
University of California at Los Angeles, CA 90095

David J. Forliti[2]
Sierra Lobo, Inc. supporting AFRL/RQRC, Edwards AFB, CA 93524

Ivett A. Leyva[3]
AFRL/RQRE, Edwards AFB, CA 93524

and
Douglas G. Talley[4]
AFRL/RQRC, Edwards AFB, CA 93524

An experimental study has been conducted at the Air Force Research Laboratory at Edwards Air Force Base to explore the receptivity of cryogenic coaxial jet flows to transverse acoustic disturbances. The shear coaxial jet flow employed liquid nitrogen in the inner jet and cooled helium in the outer annular jet to represent the nominal fluid dynamical conditions of an oxygen/hydrogen liquid rocket engine injector. The injector flow is submerged in a chamber that experiences a monotonic transverse acoustic resonance characteristic of a rocket chamber in the presence of combustion instability. The coaxial jet is exposed to a variety of acoustic conditions including different frequencies, amplitudes, and locations within the resonant mode shape. High-speed back-lit images were captured to record the behavior of the natural (unforced) and forced coaxial jets. Proper orthogonal decomposition and spectral analysis were used to extract natural and forced modes. Convective modes are extracted, and a new Strouhal number is used to characterize the dominant natural convective mode that is analogous to the preferred mode in free jets. The threshold of receptivity was found for a number of different injector flows and acoustic forcing conditions. The results indicate that the dimensionless frequency plays an important role, and there exists a finite forcing amplitude at which the threshold of receptivity occurs. The receptivity threshold and post receptivity response provides useful insight on the suitability of a given injector design for specific rocket combustion chamber conditions.

---

[1] Graduate Student, Department of Mechanical and Aerospace Engineering, UCLA, Los Angeles, CA 90095 student member. Currently at Physical Sciences, Inc., Andover, MA 01810.
[2] Research Scientist, Sierra Lobo, Inc., 10 E. Saturn Blvd, Building 8451, Edwards AFB, CA 93524, senior member.
[3] Technical Advisor, AFRL/RQRE, 4 Draco Drive, Building 8351, Edwards AFB, CA 93524, Associate Fellow.
[4] Lead, Combustion Dynamics Group, AFRL/RQRC., 10 E. Saturn Blvd, Building 8451, Edwards AFB, CA 93524, Associate Fellow.

Nomenclature

AR	=	outer-to-inner area ratio
c	=	speed of sound
D	=	diameter
f	=	frequency
F	=	normalized frequency
J	=	outer-to-inner momentum flux ratio
m	=	mass
p	=	pressure
p'	=	pressure fluctuation amplitude
St	=	Strouhal number
t	=	inner jet post thickness
U	=	mean velocity
u'	=	velocity fluctuation amplitude
ρ	=	density

Subscripts

c	=	convection
meas	=	measured
Dimotakis	=	the Dimotakis[1] convection velocity model
1	=	inner jet fluid
2	=	outer jet fluid

I. Introduction

COMBUSTION instability phenomena has been and remains one of the key challenges in the development of robust and high performance propulsion and energy systems. In the liquid rocket engine (LRE) application, combustion instability can lead to degraded performance, severe wear, and rapid catastrophic damage to the propulsion system. Unfortunately, combustion instability phenomena are not sufficiently understood to allow solution at the engine design stage. Thus full-scale testing and potential multiple design iterations may be required to satisfy the stability requirement. The development of high-fidelity design tools offers much promise in this respect, although data under a variety of relevant conditions are still needed to validate emerging computational tools.

The Air Force Research Laboratory (AFRL) at Edwards AFB has extensively investigated the mixing properties of cryogenic single and coaxial jets under both sub- and supercritical thermodynamic pressure operating conditions.[2, 3] These flows have also been exposed to a range of transverse acoustic conditions.[4-6] A new experimental facility for reacting coaxial jet flows has been developed as described by Wegener et al.[7] The present paper describes preliminary nonreacting data that was collected using this new facility. Although a large quantity of data has been collected in the past for nonreacting conditions, the current data considers a new framework in which to explore the forcing response of coaxial jets. Past studies have generally placed emphasis on investigating different injector conditions, including injector geometry, momentum flux ratio, and chamber pressure. The current study focuses on a single injector geometry in a two-phase (i.e. subcritical) regime, and focuses on the role of forcing frequency and amplitude.

II. Background

The free jet is known to contain a broad range of frequencies, ranging from the shear layer instabilities near the nozzle exit, to the large-amplitude fluctuations near the end of the potential core, and continuing into the weak far field fluctuations.[8-11] Although the global spectral features of the free jet are extremely broad band, the peak frequencies near the end of the potential core are generally selected as being a representative characteristic of the jet.[8] The approach adopted by Birbaud et al. is also highly appropriate in selecting two frequencies that represent the near field ranging from the nozzle trailing edge to the end of the potential core.[12] Having one (or more) characteristic frequency provides a useful reference in which to examine the effects of forcing, as different relative frequencies will influence the jet/shear layer structure through different mechanisms.

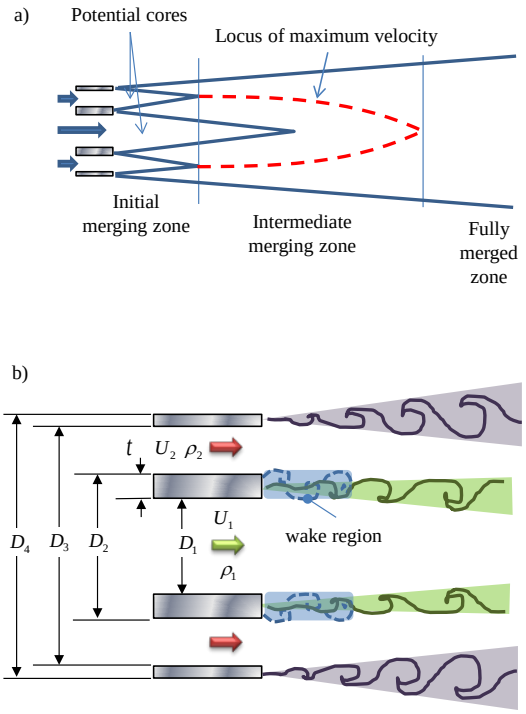

Figure 1. The a) spatial regions of the coaxial jet flow field and b) the potential unsteady structure in the initial merging zone.

The coaxial jet is a highly complex flow due to the presence of multiple shear layers and potentially a splittler plate wake instability in the near field as shown in Fig. 1. Figure 1(a) shows the spatial development of the coaxial jet as described by Ko and Kwan.[13] Figure 1(b) shows the potential shear flow regions in the initial merging zone including an inner and outer shear layer, and a possible wake instability associated with the flow downstream of the inner nozzle trailing edge. This wake instability has been found to occur within certain velocity ratio ranges for coaxial jets and shear layers.[14-20] The role of density ratio on the competition between the shear layer and wake modes has not been thoroughly explored, in particular in the small density ratio (outer to inner stream) regime associated with the conditions of interest at AFRL.

Ko and coworkers have studied the flow and spectral properties of coaxial jets spanning a broad range of conditions.[13, 21-23] They employed two different Strouhal number definitions for the inner and outer shear layer. The inner shear layer Strouhal number definition compensates for the presence of the outer flow, which has a tendancy to increase the frequency through a higher instability convection velocity. For the application of interest at AFRL, the frequencies in the inner shear layer region are of primary interest, as this will be the location of the flame under reacting flow conditions. Thus hydrodynamic instabilities in this region are most likely to generate coherent heat release fluctuations that are known to participate in thermoacoustic instability mechanisms. In this context, a representative preferred mode of the coaxial jet would be be based on the frequency of the inner shear layer structures (which may be dominated by the wake instability) near the end of the inner jet potential core where fluctuations are most intense. Although this preferred mode is likely to generate heat release fluctuations, one must remain cognizant that higher frequency fluctuations closer to the injector trailing edge might play a very key role in driving combustion instability. This aspect will be a subject of future reacting flow research at AFRL.

The coaxial jet flow is dependent on a large number of dimensionless groups. The geometry can be characterized by the outer-to-inner area ratio *AR*, and the normalized post thickness t/D_1. There are two Reynolds numbers, one each for the inner and outer flow. The momentum flux ratio *J*, defined outer to inner flow, is generally considered the primary independent flow parameter of the coaxial jet. Each of the two flows have characteristic velocities and densities, allowing the ability to define the velocity and density ratio across each shear layer. The shear flow is also very sensitive to the injector exit conditions, including profiles of mean and fluctuating velocity, and spectral characteristics of turbulence or other background disturbances. If the two streams differ in phase, then the Weber number is also a parameter of importance.

The behavior of the acoustically-excited coaxial jet will depend on all of the parameters mentioned above, in addition to the characteristic scales of the forcing conditions. The forcing can be characterized by the acoustic frequency and amplitude; the amplitude may be measured by the magnitude of the pressure and/or velocity fluctuations. The interaction mechanisms differ when the coaxial jet is placed in a fluctuating pressure environment versus a fluctuating velocity environment.[24] Thus the response of a given coaxial jet flow to acoustic perturbations will depend on the relative frequency, relative amplitude, and location within the acoustic resonance mode shape.

The purpose of the current study was to explore the receptivity of cryogenic two-phase coaxial jets to disturbances of the form of an acoustic transverse resonance; a flow is considered to be receptive to perturbations if detectable changes occur in the flow field. This study considered new parameters, the normalized frequency and amplitude. The conditions at which forcing dominates the natural coaxial jet behavior were documented.

III. Experimental facility and methods

The experiments were conducted in the Combustion Stability Lab at the Air Force Research Laboratory (AFRL) at Edwards Air Force base. A new facility, capable of high-pressure reacting flows, was used for the current study. Figure 2 shows both a schematic and three-dimensional rendering of the test chamber. Two acoustic sources, piezo sirens from Piezo Systems, Inc., are located symmetrically offset from the injector region. Waveguides shown in Fig. 2(a) are used to connect the acoustic sources to the injector flow region. The acoustic frequency and amplitude are controlled via a signal generator/amplifier combination that drives the sirens. The sirens operate either in phase or with 180° shift to generate the pressure antinode (PAN) and pressure node (PN) at the middle of the chamber; the pressure node case is associated with an acoustic velocity antinode, but will be referred to as pressure node.

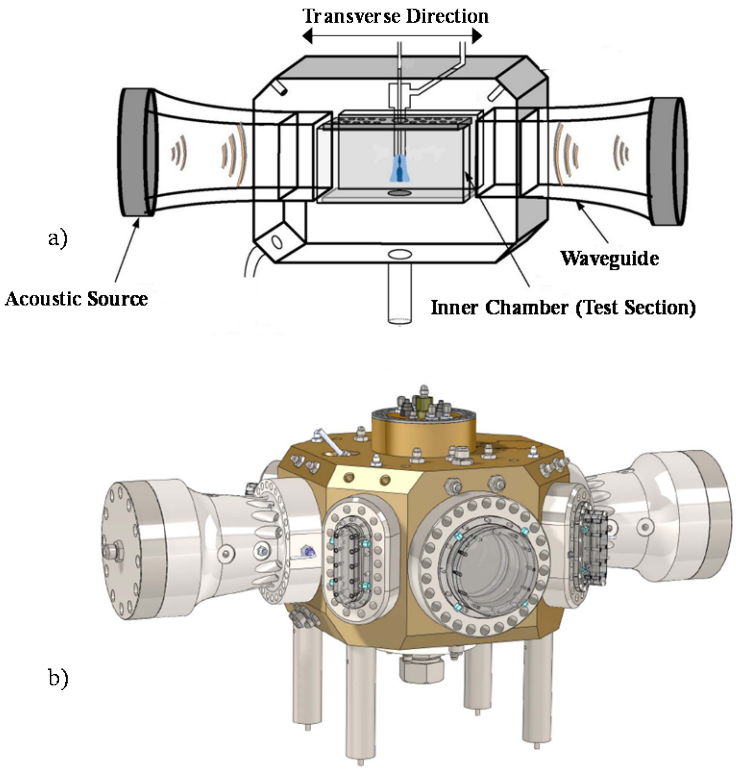

Figure 2. a) Conceptual and b) schematic of the Combustion Stability Lab experimental facility.

The chamber is divided into inner and outer chambers that are not completely sealed relative to one another. A high flow of gaseous nitrogen in the outer chamber is used to cool the combustion products under reacting flow conditions, and the combined flow is choked through an exit orifice. The gaseous nitrogen flow is used to control the chamber pressure. The facility is equipped with heat exchangers to allow cooling of the inner and outer injector flows. Further details on the experimental facility can be found in Wegener et al.[7]

Table 1. Geometry of the injector.

Parameter	Value (mm)
D_1	1.40
D_2	2.16
D_3	2.82
D_4	3.56

A single coaxial jet injector was used for the experiments. The dimensions of the injector are summarized in Table 1. The outer-to-inner area ratio *AR* is 1.68 and the dimensionless post thickness t/D_1 is 0.27; both parameters are within the lower range of previous studies at AFRL.[4, 6] The injector flow passages are sufficiently long to ensure fully-developed turbulent flow at the exit of the injector. Similar to previous work at AFRL, the inner jet is liquid nitrogen. The outer jet in the current study is cooled helium. The use of helium allows for a closer match to the density ratio as would occur for oxygen/hydrogen operation in a cryogenic rocket engine. The chamber pressure was 2.8 MPa (400 psi) for all experiments. Further details on the experimental conditions are given in Table 2.

Table 2. Injector operating parameters.

Parameter	Values
T of inner jet (N_2)	~ 120 K
T of outer jet (He)	~ 275 K
J	2, 6
Re_1	~$1.5x10^4$
Re_2	~ $1.0x10^4$
We	> 100

As shown in the table, two momentum flux ratios were considered. Due to the unique combination of fluids and conditions, surface tension values are not available to the authors' knowledge. Based on the visualizations shown later and the results of Farago and Chigier[25], the current experiments appear to be in the fiber-type regime and the Weber number is expected to be approximately 100 or higher.

The primary diagnostic of the current experimental study involves high-speed backlit imaging. A Phantom v7.10 camera was used to capture images at 10 kHz. The acoustic resonance is characterized through several high-

speed Kulite pressure sensors flush mounted in the test section area including the waveguides. A pressure sensor located in the center of the test section and coincident with the axis of the coaxial jet is used to measure the peak pressure fluctuation for the PAN cases. For the PN operation, the peak pressure fluctuation is estimated from measurements at off-node locations using an assumed mode shape, and the maximum acoustic velocity magnitude is estimated from the linear acoustics equation,

$$u' = \frac{p'}{\rho_c c} \tag{1}$$

where *u'* is the magnitude of the velocity fluctuation in the velocity antinode region, *p'* is the magnitude of the pressure fluctuation in the pressure antinode region, ρ_c is the density of the ambient gas in the chamber, which is nominally room temperature nitrogen, and *c* is the speed of sound. The injector flow species and temperatures will definitely alter the properties of the acoustic resonance, thus Eq. (1) is an approximation. The acoustic sirens were used to drive a transverse acoustic resonance ranging from the 3rd to 7th mode. See Wegener et al. for more details on the acoustic characteristics.[7]

IV. Results

The first phase of the research was focused on understanding the properties of the unforced coaxial jet. Figure 3 shows instantaneous and mean images of the cryogenic coaxial jet at the two momentum flux ratios *J* of two and six.

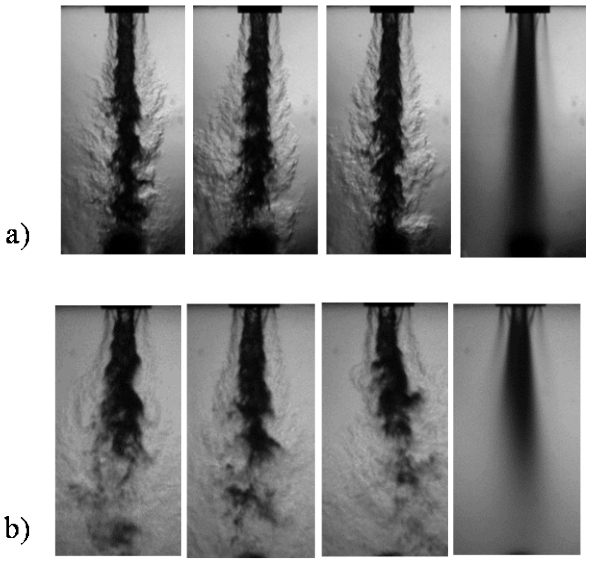

Figure 3. Instantaneous and mean (far right) backlit images of the coaxial jet for momentum flux ratio *J* of a) two and b) six.

Although there are dynamics present in both the inner and outer shear layers, the strong contrast between the liquid inner flow and gaseous outer flow dominates the images. One can see some structure within the inner shear layer, although the turbulent inflow conditions result in a highly disturbed interface between the liquid and gas. As expected, the higher momentum flux ratio case has a shorter dark core length.[26] The triangular feature near the injector exit, more readily seen in the $J = 6$ case, is the recirculation zone downstream of the inner tube post. Some asymmetries are also apparent and are caused by manufacturing tolerances and the small scale of the injector components. Separate analyses of each side of the injector flow field indicate similar spectra content (see Wegener[27] for details). It is thus expected that the general trends of the current results are representative of the symmetric case, although this will be validated in future studies.

As mentioned earlier, there is a need to identify the preferred mode of the coaxial jet. A frequency scaling variable, the Strouhal number, may be developed for use in a preferred mode scaling law. There are a number of choices available in defining the length and velocity scale for the Strouhal number. The length scale is a relatively straightforward choice of jet diameter as used for the single jet. In the case of a coaxial jet with finite (or large) post thickness t/D_1, previous studies show, at least for moderate to high *J*, that the shear layer will more or less be centered near the middle of the post.[6] Thus the average of D_1 and D_2 are used as the length scale. Further data would need to be considered for different geometries to find the length scale that provides the best collapse across different injector designs.

The velocity scale is more subjective. For the free jet, the convention is to use the mean jet exit velocity. Guidance for an alternative choice is provided through studies of shear layers. Huerre and Monkewitz conducted a linear stability study of variable velocity ratio shear layers.[28] They found that the most unstable frequencies nominally collapse on a single value when the frequency is normalized by the mean velocity of the two streams. For variable density shear layers, the frequency of the most unstable mode will more likely scale with the convection velocity. Thus the convection velocity is proposed as an appropriate velocity scale.

The convection velocity of the coherent structures in a shear layer may be estimated in a variety of ways. Linear stability analysis may be used, for instance. Dimotakis developed a model for the spreading rate of planar shear layers, and included in the model development is an estimate of the convection velocity based on freestream conditions.[1] The model uses the assumption that in the reference frame of the shear layer structure, the dynamic pressures of the two freestreams are equal. This leads to a form of the convection velocity of

$$U_{c,\,Dimotakis} = \frac{\rho_1^{1/2} U_1^2 + \rho_2^{1/2} U_2^{1/2}}{\rho_1^{1/2} + \rho_2^{1/2}}, \tag{2}$$

where ρ and U are the density and velocity of the freestreams. It should be mentioned that this expression was derived for single-phase shear layers.

In order to evaluate the validity of the Dimotakis model, the convection velocity is directly measured from the time-resolved images. Figure 4(a) shows the mean image for the $J = 6$ case. A line along the middle of the inner shear layer is defined through user input, and the intensities of these pixels are plotted as a function of time as shown in Fig. 4(b). As inner fluid structures convect along this trajectory, they trace diagonal lines in the s/D_1 versus time domain. This technique has been used in the past to visualize organized motion in jets.[29] The slope of a particular diagonal line represents the convection velocity for that structure; s is the distance along the shear layer ray. Ten samples are extracted and the mean convection velocity determined. The change in slope near s/D_1 of unity is coincident with the end of the triangular recirculation zone associated with the blunt post wall. As expected, the convection velocity increases downstream of the recirculation zone due to the presence of the high-speed coflow of the outer jet fluid; the outer-to-inner velocity ratio for this case is 25. This convection velocity analysis was conducted for several sets of data including two momentum flux ratios and two flow rate combinations.

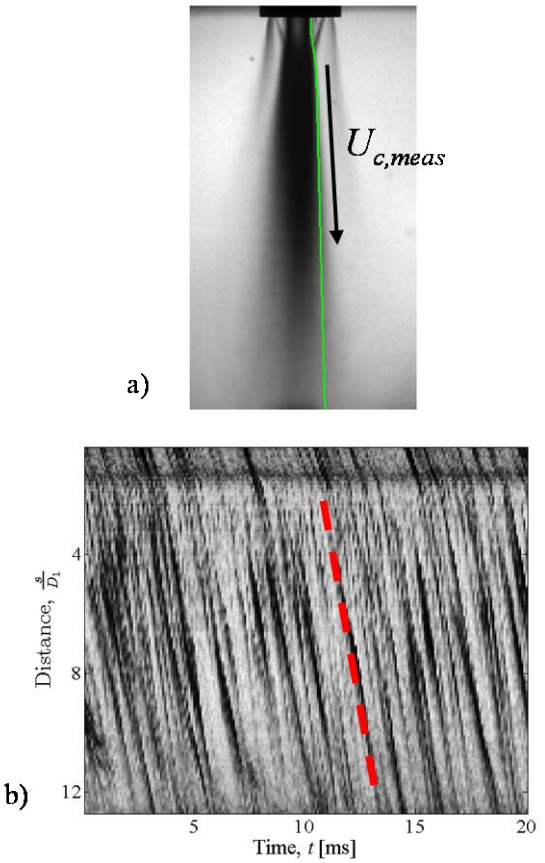

Figure 4. The (a) piecewise linear domain used to construct the (b) axial versus time maps for evaluating the convection velocity.

Figure 5 shows predicted versus measured convection velocities for the two momentum flux ratios. Data was collected for nominal and a higher flow rate for both momentum flux ratios. The conditions for the two momentum flux ratios were selected to keep the convection velocity predicted using Eq. (2) fixed, hence the overlap of points for both momentum flux ratios. The agreement is quite good, indicating that the Dimotakis model may be employed for the current flow conditions. A deviation is observed at higher flow rates (i.e. high convection velocities) and is likely due to heat transfer within the injector. Measurement of temperatures upstream of the injector is used to evaluate density for both flows, thus errors in temperature will result in errors in density. The velocity is estimated using the calculated density and the measured flow rate, thus creating further error due to temperature uncertainty. The subsequent measurements were all done at the lower flow rate associated with a convection velocity near 6 m/s.

In order to calculate the Strouhal number, the characteristic frequency of the jet must be extracted from the data. As would be expected for a spreading shear flow, the spectra depend on axial position. The global frequency of the jet is evaluated using proper orthogonal decomposition (POD) of the image data. This approach places more emphasis on the larger-scale organized motions which make higher contributions to the total variance of the data, thus will be biased towards dynamics in the downstream region. The POD is calculated for an image that spans an

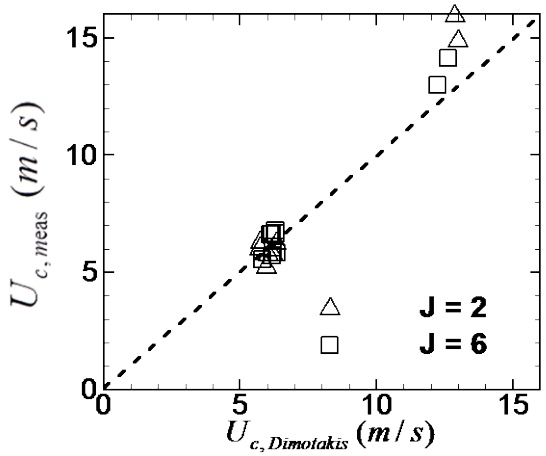

Figure 5. Measured versus predicted convection velocity.

axial distance of approximately $12D_1$. The POD is calculated using singular value decomposition (SVD), the details of which can be found in Wegener.[27] The POD is applied to sets of 2000 images.

The application of POD to 2000 images yield the same number of variance-contributing modes, thus the POD spectrum is inherently broadband, especially for highly-turbulent flows of the type in the present study. Thus a criteria must be defined for isolating important dynamics from the POD results. Arienti and Soteriou provide a criteria for identifying convective modes from POD data.[30] First, the POD spectrum, meaning the eigenvalues as a function of mode number, is constructed and pairs of modes with similar eigenvalues are sought. Once a candidate mode pair is identified, the cross-power spectral density (CPSD) amplitude and phase are calculated for the temporal coefficients of the mode pair. Once this has been done, the mode pair can be determined to be representing a convecting mode if:

1. the peak in the CPSD is coincident with a region of ± 90° phase shift;
2. the spatial distribution of the POD eigenfunctions are similar with features that are shifted nominally half a wavelength in the convection direction.

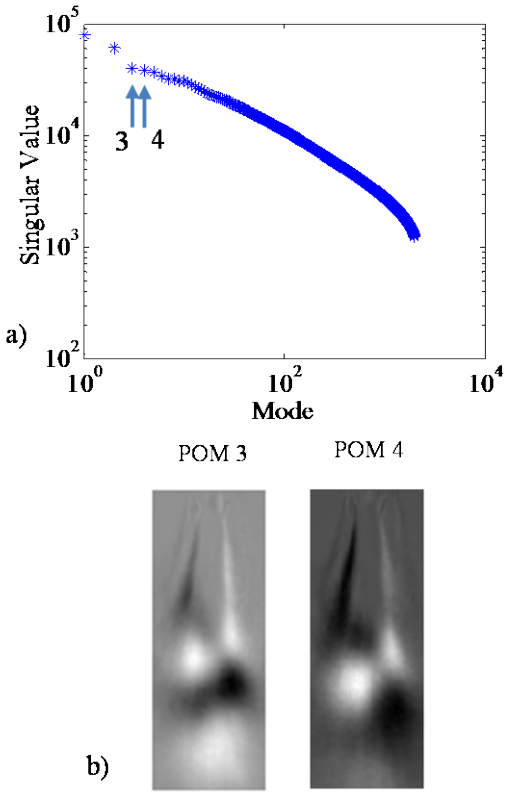

Figure 6. Proper orthogonal decomposition a) spectrum and b) eigenfunctions of mode pair candidate proper orthogonal modes (POM) three and four for J = 2.

If a mode pair satisfies these conditions, a convective dynamic mode has been identified and the frequency of the particular convective mode is associated with the peak in the CPSD. In this study, the preferred mode is associated with the convective mode having the most energetic POD mode pair (i.e. has the highest eigenvalues). The singular values from the SVD process are used to evaluate the variance, as the singular values are equal to the square root of the eigenvalues. It is likely that multiple convective modes are present in the unforced cases of the present study. Other convective modes with lower singular values are not considered as representing preferred modes.

Figure 6(a) shows an example of a POD spectrum (in terms of singular values) as a function of mode number. The most energetic mode pair with similar singular values is associated with modes three and four. Figure 6(b) shows the proper orthogonal modes (POMs), or eigenfunctions, associated with the mode pair. This figure shows that the spatial distribution is similar, while mode four appears to have features that are slightly shifted downstream relative to mode three. Reconstructing these two modes with the temporal coefficients will represent a convective process. It may be seen that modes seven through nine also have similar singular values, thus a second convective mode may be present. This mode was not evaluated due to the lower variance contribution.

Figure 7 shows the CPSD and phase difference for modes three and four shown in Fig. 6. There is a broad peak on the low-frequency side of the spectrum. The peak is defined within the broad CPSD peak but also requires the phase to be near ± 90°. The frequency is near 1 kHz.

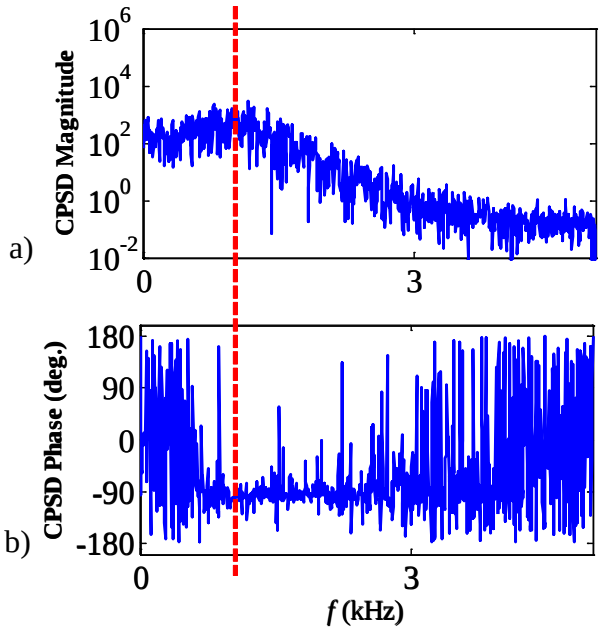

Figure 7. Cross-power spectral density a) amplitude and b) phase for modes three and four for J = 2.

The process described above to identify the preferred mode frequency of the coaxial jet was applied to a number of data sets for both momentum flux ratios and nominal and high flow rates. The Strouhal number defined as

$$St = \frac{f_{nat}(D_1 + D_2)/2}{U_{c,meas}}, \tag{3}$$

where f_{nat} is the preferred mode frequency, was calculated for all data sets. The Strouhal number as a function of momentum flux ratio is shown in Fig. 8. The measured convection velocity provides a slightly reduced level of scatter compared results using Eq. (2). The trend represents a nominally constant value for St of 0.3. Spectra near the potential core end for the free jet data of Ko and Davies[9] and coaxial jet data of Ko and Kwan[13], when recast in the form of Eq. (3), fall within the scatter around 0.3. Both nominal and higher flow conditions (i.e. higher convection velocities) fall nominally near 0.3.

The scaling law in Fig. 8 was used to define baseline flow conditions for a predetermined frequency. Since the geometry is fixed, the preferred mode is governed by the convection velocity. For the present study, the unforced flow conditions were defined to result in a preferred mode frequency of approximately 1 kHz.

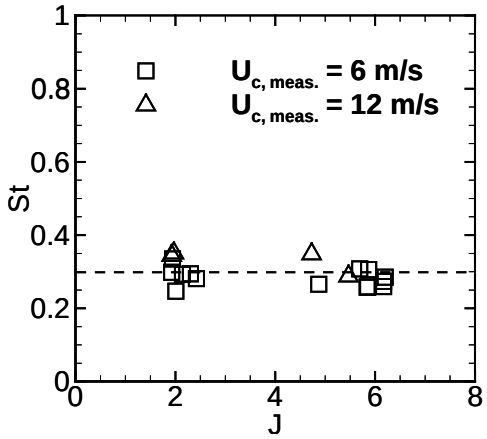

Figure 8. Strouhal number versus momentum flux ratio J.

One of the primary forcing parameters is the frequency ratio F, defined as

$$F = \frac{f_{forcing}}{f_{nat}}, \tag{4}$$

where $f_{forcing}$ is the forcing frequency and f_{nat} is the natural preferred mode. The current study considered frequency ratios near 1.7, 2.0, and 2.6. The amplitude normalization will be discussed for both the PAN and PN forcing conditions.

Figure 9 shows instantaneous images of the J = 2 case for baseline and max PAN/PN forcing. The outer flow and inner shear layer are clearly perturbed under forcing conditions. In particular, the PN forcing results in highly antisymmetric structure in the outer annular flow with antisymmetric structures on the inner jet boundary. The instantaneous image for the PAN case shows large-scale structures on the inner jet surface, while it is not apparent whether the structure is symmetric or antisymmetric.

One of the primary goals of the research was to identify the conditions of forcing receptivity as a function of dimensionless forcing frequency and amplitude. The POD technique is used to detect the receptivity and relative importance of the forced and natural modes. Figure 10 shows the first eight POMs for the baseline unforced case, and two forcing amplitudes of 1.15 and 1.88 psi for the PAN case for J = 2.0 and F = 2.6. The dashed blue box represents the natural preferred mode, which is present for all cases. The p' = 1.15 psi case shows the emergence of a new high frequency convective mode pair for modes 7 and 8. This force mode is highlighted by the red dashed box. When the amplitude was increased to 1.88 psi, the forced mode contributes more to the image variance as indicated by the order within the POD array. For the forced dominated case in Fig. 10(c), the natural mode persists but is somewhat contaminated with small-scale instabilities from the forcing.

For PAN forcing, the injector is essentially exposed to an unsteady back pressure. Thus the coupling is likely to be related to unsteady flow rates caused by a fluctuating pressure drop across the injector. Due to the high density

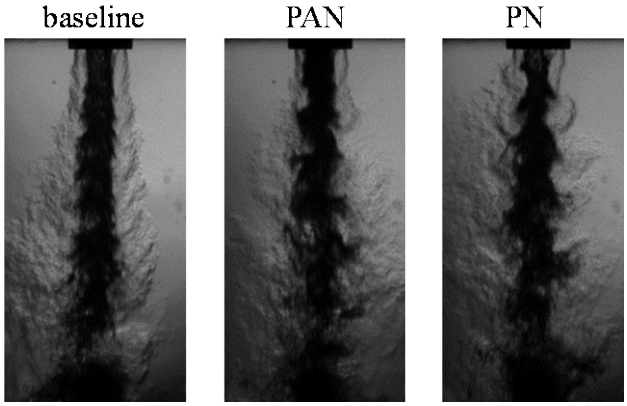

Figure 9. Instantaneous images for the baseline and maximum forced cases for PAN and PN, J = 2.

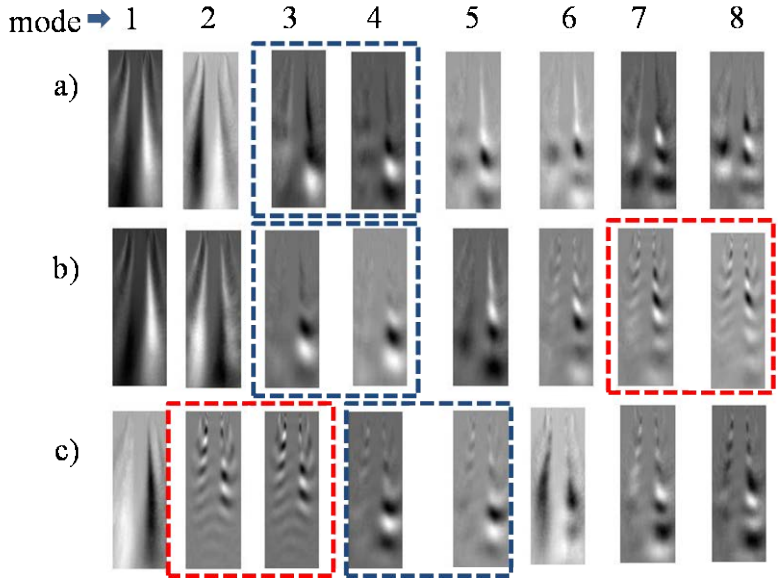

Figure 10. Proper orthogonal modes for J = 2, PAN, and F = 2.7 for a) unforced, b) p' = 1.15 psi, and c) p' = 1.88 psi.

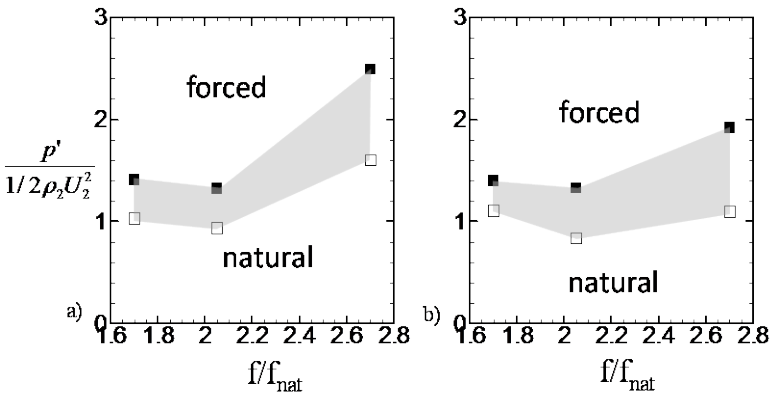

Figure 11. Receptivity regimes for PAN forcing as a function of frequency ratio for a) J = 2 and b) J = 6.

of the inner jet, the impact of the unsteady pressure drop is reduced because of the high inertia within the injector passage. The outer jet is much more responsive to the unsteady back pressure due to the lower mass in the outer jet passage. Thus fluctuating back pressure drives a fluctuating flow rate in the outer jet. The accompanying velocity pulsations will disturb both the inner and outer shear layer. This description is consistent with the explanation given by Baillot et al.[24]

The above mechanism provides for some guidance for normalization of the forcing amplitudes for PAN conditions. The unsteadiness generated in the outer flow will depend on the ratio of the unsteady back pressure to the dynamic pressure of the flow. The magnitude of the induced velocity fluctuation will also depend on the frequency (see Wegener[27] for analysis). For a fixed pressure drop across the injector passage, high-frequency fluctuations have a shorter time period in which the fluid can accelerate. Thus it is expected that higher-frequency fluctuations are less likely to couple for PAN forcing, although the hydrodynamic stability considerations also play a factor in how velocity fluctuations of a particular frequency lead to wrinkling of the inner jet column.

Figure 11 shows the inception and dominance boundaries of the PAN forcing conditions for both momentum flux ratios at the three frequency ratios. The empty symbols represent the conditions in which a new forced POM mode pair was observed, but was lower in variance contribution than the natural mode. The filled symbol represents the condition in which the forced mode is dominant over the natural mode. Other test points above and below these points are not included for clarity. Between five and seven amplitudes were tested for each frequency ratio. The grey shaded area has not been sampled, although the transition between natural and forced dominance occurs in this region.

It is interesting to note that the inception of receptivity occurs at a nominal dimensionless

amplitude of unity. This is consistent with the arguments of Baillot et al.[24] It is unclear why the $J = 2$ case appears to be less receptive to high-frequency fluctuations, both in terms of initial detection of receptivity and the amplitude required for the force mode to dominate the natural mode. The $J = 6$ case appears to be less sensitive to frequency ratio in the range explored.

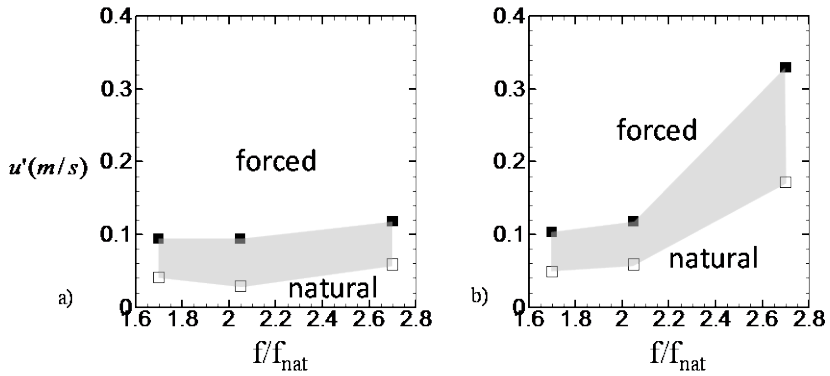

Figure 12. Receptivity regimes for PN forcing as a function of frequency ratio for a) $J = 2$ and b) $J = 6$.

Figure 12 shows the receptivity behavior for the PN forcing conditions. Here the amplitude of the forcing is given in units of m/s. The perturbation velocity is estimated using Eq. (1). The general trend of increasing receptivity with amplitude is once again demonstrated. The mechanism for the response is less evident. The velocity perturbation magnitude is much lower than the outer jet velocity (~ 40 m/s). It is thus unlikely that the perturbations are directly disturbing the inner jet surface as these low-level disturbances would be insignificant relative to the inflow turbulence. Interestingly, the higher momentum flux ratio case exhibits stronger frequency dependence including degraded receptivity at high frequency.

Further insight may be gained through analysis of the images in the first few diameters of the coaxial jet. In this region, the flow is very unstable due to the high velocity gradients, thus this is the most likely region where the acoustic perturbations can disturb the flow. Figure 13 shows the near field of the coaxial jet for the baseline

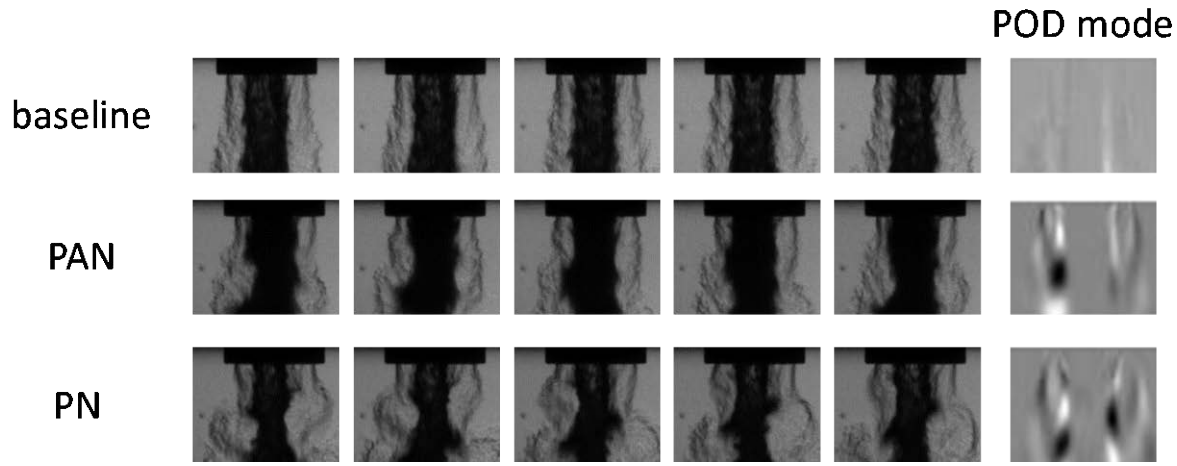

Figure 13. Instantaneous images of the near field of the coaxial jet under forced and unforced conditions for $J = 2$.

unforced case as well as highly-forced PAN and PN cases. These images are also representative for the results at $J = 6$. The near field of the dominant convective POM modes are also shown on the right of the figure. The PAN mode, as supported by the POM distribution, is symmetric (although the thickness and intensity is not symmetric). This would be supportive of the pulsed outer flow mechanism, although this is not nearly as clear in the instantaneous images. The PN case shows very dramatic effects in the near field. In particular, the outer jet appears to be experiencing intense transverse motions that are out of phase. The antisymmetric nature is also supported by the POM. Recall from Fig. 12 that the estimated acoustic velocity is much smaller than the outer jet velocity. The flapping nature of the jet, and the involvement of the jet as a whole, suggests the possibility of excitation of a helical jet column mode (or multiple modes). The transverse velocity disturbance is not of sufficient magnitude to cause a

drag force leading to such dramatic motion. Future analysis will be required to gain further insight into the coupling mechanism for PN conditions.

V. Conclusions

An experimental study has investigated the receptivity of two-phase coaxial jet flows to transverse acoustic perturbations. It was found, over the range of conditions considered, that the shear flow structures along the inner jet convect at a speed well predicted by the model developed by Dimotakis.[1] A new Strouhal number definition is proposed that appears to provide reasonable collapse of the frequency of convective modes as extracted from POD analysis of the potential core region of the coaxial jet. Coaxial jets at two different momentum flux ratios were subsequently forced through exposure to variable frequency and amplitude acoustic environments, including pressure node and pressure antinode conditions.

The pressure antinode forcing appears to generate a pulsation in the outer jet flow rate that subsequently excites instabilities in the flow. The receptivity of the flow field to pressure antinode forcing occurs near the condition where $p' \sim 1/2 \rho_2 U_2^2$, independent of momentum flux ratio, with the exception of highest frequency case for $J = 2$. This mechanism will also be sensitive to the inertance properties of the injector design, and therefore sensitive to frequency. The receptivity charactersitics are different for the two momentum flux ratios, even though the frequency of the preferred modes were the same. This suggests more subtle differences in the hydrodynamics between the two momentum flux ratios play a role in the receptivity characteristics.

The pressure node forcing results in a strong coupling even at very low acoustic velocities. The relative magnitudes of the acoustic velocity to the characteristic velocities of the coaxial jet make it unlikely that the acoustics directly generate disturbances in the shear flow. A potential mechanism involves the coherent transverse velocity fluctuations in the acoustic field exciting one or multiple helical modes in the outer jet. Further research will be required to further explore the coupling mechanism for pressure node forcing. Once again, the receptivity trends were different for the two momentum flux ratios, suggesting again the presence subtle hydrodynamic effects in the receptivity mechanism. Interestingly, the lower momentum flux ratio case is less receptive at high frequency for the pressure antinode forcing while the higher momentum flux ratio case is less receptive for the pressure node forcing.

Acknowledgments

Support was provided by the Air Force Office of Scientific Research, project officer Mitat Birkan, and by AFRL Laboratory Revitalization Funds. The authors thank Randy Harvey and Todd Newkirk for their assistance in conducting the experiments.

References

1. Dimotakis, P. E., "Two-dimensional shear-layer entrainment," *AIAA Journal*, Vol. 24, No. 11, 1986, pp. 1791-1796.

2. Chehroudi, B., Talley, D., and Coy, E., "Visual characteristics and initial growth rates of round cryogenic jets at subcritical and supercritical pressures," *Physics of Fluids*, Vol. 14, No. 2, 2002, pp. 850-861.

3. Oschwald, M., Smith, J., Branam, R., Hussong, J., Schik, A., Chehroudi, B., and Talley, D., "Injection of fluids into supercritical environments," *Combustion Science and Technology*, Vol. 178, No. 1-3, 2006, pp. 49-100.

4. Davis, D. W., "On the behavior of a shear-coaxial jet, spanning sub-to supercritical pressures, with and without an externally imposed transverse acoustic field," Ph.D., Mechanical Engineering, The Pennsylvania State University, 2006.

5. Rodriguez, J. I., "Acoustic excitation of liquid fuel droplets and coaxial jets," Ph.D., Aerospace Engineering, University of California, Los Angeles, 2009.

6. Teshome, S., "Droplet Combustion and Non-Reactive Shear-Coaxial Jets with Transverse Acoustic Excitation," Ph.D., Mechanical Engineering, University of California, Los Angeles, 2012.

7. Wegener, J., Leyva, I., Forliti, D., and Talley, D., "Development of a facility for combustion stability experiments at supercritical pressure," 52nd AIAA Aerospace Sciences Meeting, National Harbor, MD, 2014.

8. Crow, S., and Champagne, F., "Orderly structure in jet turbulence," *Journal of Fluid Mechanics*, Vol. 48, 1971, pp. 547-591.

9. Ko, N., and Davies, P., "The near field within the potential cone of subsonic cold jets," *Journal of Fluid Mechanics*, Vol. 50, No. 01, 1971, pp. 49-78.

10. Yule, A. J., *Two-dimensional self-preserving turbulent mixing layers at different free stream velocity ratios*, Aeronautical Research Council 1972.

11. Drubka, R. E., and Nagib, H. M., "Instabilities in near field of turbulent jets and their dependence on initial conditions and Reynolds number," *AFOSR Scientific Report AFOSR-TR-0962*. 1981.

12. Birbaud, A.-L., Durox, D., Ducruix, S., and Candel, S., "Dynamics of free jets submitted to upstream acoustic modulations," *Physics of Fluids*, Vol. 19, 2007, p. 013602.

13. Ko, N., and Kwan, A., "The initial region of subsonic coaxial jets," *Journal of Fluid Mechanics*, Vol. 73, 1976, pp. 305-332.

14. Boldman, D., Brinich, P., and Goldstein, M., "Vortex shedding from a blunt trailing edge with equal and unequal external mean velocities," *Journal of Fluid Mechanics*, Vol. 75, 1976, pp. 721-735.

15. Segalini, A., and Talamelli, A., "Experimental analysis of dominant instabilities in coaxial jets," *Physics of Fluids*, Vol. 23, No. 2, 2011, pp. 024103-1-024103-7.

16. Talamelli, A., and Gavarini, I., "Linear instability characteristics of incompressible coaxial jets," *Flow, Turbulence and Combustion*, Vol. 76, No. 3, 2006, pp. 221-240.

17. Talamelli, A., Segalini, A., Örlü, R., and Buresti, G., "A note on the effect of the separation wall in the initial mixing of coaxial jets," *Experiments in Fluids*, Vol. 54, No. 3, 2013, pp. 1-7.

18. Tian, V., McKeon, B., and Leyva, I. A., "Split stream flow past a blunt trailing edge with application to combustion instabilities," 46th AIAA/ASME/SAE/ASEE Joint Propulsion Conference and Exhibit, 2012.

19. Wallace, D., and Redekopp, L., "Linear instability characteristics of wake-shear layers," *Physics of Fluids A: Fluid Dynamics*, Vol. 4, No. 1, 1992, pp. 189-191.

20. Sarpotdar, S., and Raman, G., "Investigation of the Inner Nozzle Wake on Kelvin Helmholtz Instabilities in a Coannular Jet," *International Journal of Flow Control*, Vol. 3, No. 2, 2011, pp. 67-86.

21. Kwan, A., and Ko, N., "The initial region of subsonic coaxial jets. Part 2," *Journal of Fluid Mechanics*, Vol. 82, 1977, pp. 273-287.

22. Ko, N., and Au, H., "Coaxial jets of different mean velocity ratios," *Journal of Sound Vibration*, Vol. 100, 1985, pp. 211-232.

23. Au, H., and Ko, N., "Coaxial jets of different mean velocity ratios. II," *Journal of Sound Vibration*, Vol. 116, 1987, pp. 427-443.

24. Baillot, F., Blaisot, J.-B., Boisdron, G., and Dumouchel, C., "Behaviour of an air-assisted jet submitted to a transverse high-frequency acoustic field," *Journal of Fluid Mechanics*, Vol. 640, 2009, pp. 305-342.

25. Chigier, N., and Farago, Z., "Morphological classification of disintegration of round liquid jets in a coaxial air stream," *Atomization and Sprays*, Vol. 2, No. 2, 1992.

26. Leyva, I., Chehroudi, B., and Talley, D., "Dark Core Analysis of Coaxial Injectors at Sub-, Near-, and Supercritical Conditions in a Transverse Acoustic Field," 43rd AIAA/ASME/SAE/ASEE Joint Propulsion Conference & Exhibit, Cincinnati, OH, 8-11 July, 2007.

27. Wegener, J., "Multi-phase Combustion and Transport Processes Under the Influence of Acoustic Excitation," Ph.D., Mechanical Engineering, University of California, Los Angeles, 2014.

28. Monkewitz, P. A., and Huerre, P., "Influence of the velocity ratio on the spatial instability of mixing layers," *Physics of Fluids*, Vol. 25, 1982, p. 1137.

29. Dahm, W. J., and Dimotakis, P. E., "Mixing at large Schmidt number in the self-similar far field of turbulent jets," *Journal of Fluid Mechanics*, Vol. 217, 1990, pp. 299-330.

30. Arienti, M., and Soteriou, M. C., "Time-resolved proper orthogonal decomposition of liquid jet dynamics," *Physics of Fluids (1994-present)*, Vol. 21, No. 11, 2009, p. 112104.